Contribution from the Department of Theoretical Chemistry,
University of Sydney, NSW 2006, Australia

Electron Transfer and Energy Transfer through Bridged Systems. 4. Intermetallic Coupling and Electronic Spectra of the Bis(pentaammineruthenium) Complexes of α,ω-Dipyridyl *trans*-Polyenes in D_2O

J. R. Reimers and N. S. Hush*

Received October 2, 1989

The electronic spectra of all Ru^{II} and/or Ru^{III} valence states of $(NH_3)_5RuNC_5H_5$, $(NH_3)_5RuNC_5H_5-C_5H_5NRu(NH_3)_5$, $(NH_3)_5RuNC_5H_5-C_2H_2-C_5H_5NRu(NH_3)_5$, and $(NH_3)_5NC_5H_5-C_4H_4-C_5H_5NRu(NH_3)_5$ are analyzed and deconvoluted into contributions from $\pi \rightarrow \pi^*$, metal $\rightarrow$ ligand, ligand $\rightarrow$ metal, and intervalence transitions. A high degree of internal consistency is achieved, and the results are in qualitative agreement with theoretical predictions. The deduced intermetallic couplings are consistent with the theoretical prediction of a near-exponential bridge-length dependence. Predictions are made for the spectroscopy and intermetallic coupling of substituted complexes. Thermal and photoinduced electron-transfer mechanisms are compared, as are predictions for thermal electron-transfer rate constants based upon different theoretical models.

I. Introduction

The bis(pentaammineruthenium) complexes of α,ω-dipyridyl *trans*-polyenes (Figure 1) form a series of semirigid molecules in which the metal-metal separation increases almost linearly with polyene length n. As predicted by Hush[1,2] and first observed by Tom, Creutz, and Taube,[3,4] the mixed-valence $Ru^{II}-Ru^{III}$ ions display an intervalence metal $\rightarrow$ metal (M $\rightarrow$ M) transition whose intensity is related to the electronic coupling between the metal d_π orbitals. Because of the large intermetallic separation, this coupling is not due to any direct through-space overlap of the d_π orbitals but rather is due principally to a through-bridge-mediated interaction. The M $\rightarrow$ M transition is a specific example of an electron-transfer process, occurring here over large distances under somewhat controlled conditions. Long-distance electron-transfer reactions are of considerable importance in organic,[5,6] inorganic,[4,7-15] and biological[16-20] systems, as well as in molecular devices,[21-23] but too often results from these systems are difficult to interpret because of uncontrollable experimental factors such as molecular conformation. While the dipyridyl polyenes are not perfect bridging groups (they are slightly nonplanar with shallow out-of-plane torsional barriers and are thus somewhat floppy), they provide some of the best available results for the study of through-bridge electron transfer. To model such processes accurately, it is necessary to have as much information as possible about the electronic states of complexes, and thus it is desirable to extract the greatest possible information from their electronic spectra, including details of the obscured L $\rightarrow$ M bands. In this paper, we analyze the rich spectral data available for 0.1 M DCl/D_2O solution; subsequently,[24] we analyze the limited data available for nitrobenzene solution.

Ford, Rudd, Gaunder, and Taube[13] recorded the electronic spectra of the divalent and trivalent pentaammine pyridyl complexes; spectra were recorded of the $Ru^{II}-Ru^{II}$, $Ru^{II}-Ru^{III}$, and $Ru^{III}-Ru^{III}$ ions of the bis(metal) complexes for the $n = 0$ (4,4'-bipyridyl) ligand by Sutton, Sutton, and Taube,[14] for the $n = 1$ ligand by Richardson and Taube,[12,25] and for the $n = 2$ ligand by Woitellier, Launay, and Spangler.[15] Taube et al. in analyzing their spectra were concerned with determining the identity of the first M $\rightarrow$ L transition and of the intervalence M $\rightarrow$ M transition. They were not concerned with the problem of identifying and deconvoluting the overlapping L $\rightarrow$ M and $\pi \rightarrow \pi^*$ transitions. We perform this task making use of theoretical calculations of the positions and intensities of the electronic absorption bands and present a deconvolution, which while by no means being unique, provides a consistent description of the changes in the absorption bands both from complex to complex and from experiment to theory.

The theoretical model used for the electronic spectra treats the parts of the complex that are strongly coupled (such as the couplings within the ligands) at the Hartree-Fock SCF level but treats the weaker coupling between the metal d_π orbitals and the ligands with a parametrized tight-binding one-electron approach. The parameters used in this model are the metal-nitrogen coupling β_{M-N} (which is assumed constant independent of ligand, valence state, vibrational displacements, etc.) and three parameters per ligand that adjust the energies of the lowest M $\rightarrow$ M, L $\rightarrow$ M, and M $\rightarrow$ L transitions.

While this model is rather crude, it is able to interpret a large range of experimental data. Often in the study of electronic couplings in both organic and inorganic molecules, it is common to use a fully parametrized Hückel model; while such models are usually quite successful in interpreting experimental data, they are usually not transferable;[26] i.e., the parameter set that interprets one class of experimental observations is completely inappropriate for another. In terms of the interpretation of the bridge-length dependence of electronic coupling, it is possible to generate "realistic" Hückel Hamiltonians predicting decay constants covering some considerable range, including all options considered in this paper. Thus, while it is possible to use Hückel Hamiltonians

(1) Hush, N. S. *Prog. Inorg. Chem.* **1967**, *8*, 391.
(2) Hush, N. S. *Electrochim. Acta* **1968**, *13*, 1005.
(3) Creutz, C. Ph.D. Thesis, Stanford University, 1970.
(4) Tom, G. M.; Creutz, C.; Taube, H. *J. Am. Chem. Soc.* **1974**, *96*, 7827.
(5) Penfield, K. W.; Miller, J. R.; Paddon-Row, M. N.; Cotsaris, E.; Oliver, A. M.; Hush, N. S. *J. Am. Chem. Soc.* **1987**, *109*, 5061.
(6) Oevering, H.; Paddon-Row, M. N.; Heppener, M.; Oliver, A. M.; Cotsaris, E.; Verhoeven, J. W.; Hush, N. S. *J. Am. Chem. Soc.* **1987**, *109*, 3258.
(7) Mikkelsen, K. V.; Ratner, M. A. *Chem. Rev.* **1987**, *87*, 113.
(8) Stein, C. A.; Taube, H. *J. Am. Chem. Soc.* **1987**, *100*, 1635.
(9) Stein, C. A.; Taube, H. *J. Am. Chem. Soc.* **1981**, *103*, 693.
(10) Sutton, C. A.; Taube, H. *Inorg. Chem.* **1981**, *20*, 3125.
(11) Richardson, D. E.; Sen, J.; Buhr, J. D.; Taube, H. *Inorg. Chem.* **1982**, *21*, 3136.
(12) Richardson, D. E.; Taube, H. *J. Am. Chem. Soc.* **1983**, *105*, 40.
(13) Ford, P.; Rudd, D. F. P.; Gaunder, R.; Taube, H. *J. Am. Chem. Soc.* **1968**, *90*, 1187.
(14) Sutton, J. E.; Sutton, P. M.; Taube, H. *Inorg. Chem.* **1979**, *18*, 1017.
(15) Woitellier, S.; Launay, J. P.; Spangler, C. W. *Inorg. Chem.* **1989**, *28*, 758.
(16) Martin, J. L.; Breton, J.; Hoff, A. J.; Migus, A.; Antonetti, A. *Proc. Natl. Acad. Sci. U.S.A.* **1986**, *83*, 957.
(17) Breton, J.; Martin, J. L.; Hoff, A. J.; Migus, A.; Antonetti, A. *Proc. Natl. Acad. Sci. U.S.A.* **1986**, *83*, 5121.
(18) Marcus, R. A. In *Light Induced Charge Separation in Biology and Chemistry*; Gerischer, H., Katz, J. J., Eds.; Verlag Chemie: Berlin, 1979.
(19) DeVault, D. *Quantum-Mechanical Tunnelling in Biological Systems*; Cambridge University Press: Cambridge, England, 1984.
(20) Scott, R. A.; Mauk, A. G.; Gray, H. B. *J. Chem. Educ.* **1985**, *62*, 932.
(21) Reimers, J. R.; Hush, N. S. In *Moleclar Electronics-Science and Technology*; Aviram, A., Ed.; U.S. Eng. Found: New York, 1989; p 27.
(22) Reimers, J. R.; Hush, N. S. In *Electron Transfer in Biology and the Solid State*; Johnson, M. K., King, R. B., Kurtz, D. M., Jr., Kutal, C., Norton, M. L., Scott, R. A., Eds.; Advances in Chemistry Series 226; American Chemical Society: Washington, DC, 1990; p 339.
(23) Carter, F. L., Ed. *Molecular Electronic Devices II*; Marcel Dekker: New York, 1987.
(24) Reimers, J. R.; Hush, N. S. *Inorg. Chem.*, in press.
(25) Taube, H. Private communication.
(26) Salem, L. *Molecular Orbital Theory of Conjugated Systems*; Benjamin: Reading, MA, 1972.

0020-1669/90/1329-3686$02.50/0

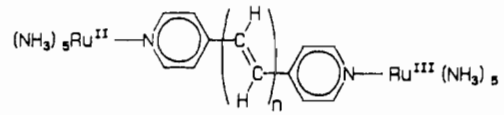

Figure 1. Bis(pentaammineruthenium) complexes of α,ω-dipyridyl *trans*-polyenes, with polyene length n.

to interpret experimental results, it is very dangerous to use them to predict the results of some different experiment. Our model, however, is designed to be *transferable*, reproducing spectroscopic transition energies and intensities of many complexes, and *predictive*, predicting values for intermetallic couplings.

Section II of this paper describes in detail the theoretical model, while section III describes the results of the deconvolution. Section IV demonstrates that the changes seen in the fitted values of the model parameters for the $n = 0$–2 ligands are consistent with CNDO predictions, while this consistency is exploited in section V to extrapolate parameters for the $n = 3$ and $n = 4$ ligands. In section VI, the intermetallic couplings deduced from the spectra are compared with those calculated from theory and the bridge-length dependence of the coupling is considered. Applications to inorganic systems with modified ligands and metals are considered in section VII with an emphasis on the prediction of complexes showing large couplings over long distances. The difference between thermal and photoinduced electron transfer is considered in section VIII, and different theoretical models for thermal electron transfer are compared with the model of photochemical electron transfer developed therein. A Hückel parametrization appropriate for this problem is described in section IX.

II. Theoretical Model

It is not possible to carry out a complete ab initio or even (without modification) an approximate valence shell calculation for these systems, since, for these ionic species, with many charge-transfer excited states, the solvent plays a critical role in determining energy levels. At present this can only be accommodated in terms of a model approach, in which energy parameters are related to experiment in an empirical manner that allows for these effects, rather than at a molecular level. The method outlined here keeps the number of such parameters to a minimum.

The theoretical model we use to obtain energy levels and eigenfunctions treats the parts of the complex that are strongly bonded (i.e., within the ligand) at the HF–SCF level. The coupling between the metal d_π orbitals and the ligand is calculated by using a parametrized tight-binding one-electron approach.

This allows the molecular orbitals of a bis(metal) complex to be obtained by diagonalizing the energy matrix

$$\underline{H} = \begin{bmatrix} \alpha_1 & \beta_{M-N} & & \\ \beta_{M-N} & & & \\ & & \underline{H}_L & \\ & & & \beta_{M-N} \\ & & \beta_{M-N} & \alpha_2 \end{bmatrix} \qquad (1)$$

where α_1 and α_2 are the energy levels of the metal d_π orbitals (these values differ according to the valence state of the metal atoms), β_{M-N} is the metal d_π to N π coupling (note that the two nitrogen π orbitals are assumed to be placed at the beginning and at the end of the ligand orbital list), and $\mathbf{H}_L$ is the ligand-only Fock matrix at self-consistency.

The energy matrix for the pyridyl complexes is obtained in a similar fashion to that of the bis(pyridyl) complexes, except that only one metal d_π orbital is added to the ligand molecular orbitals. In the following discussion, a bis(metal) complex is assumed: adaptation of the theory to pyridyl complexes is straightforward.

Let $\mathbf{C}_L$ be the matrix that transforms $\mathbf{H}_L$ to diagonal form according to

$$\mathbf{E} = \mathbf{C}^\dagger_L \mathbf{H}_L \mathbf{C}_L \qquad (2)$$

where $\mathbf{E}$ is the diagonal matrix of the ligand molecular orbital energies. The Ru–N coupling can then be given in terms of a ligand molecular orbital basis by augmenting $\mathbf{C}_L$ to produce

$$\underline{C} = \begin{bmatrix} 1 & & \\ & \underline{C}_L & \\ & & 1 \end{bmatrix} \qquad (3)$$

and transforming

$$\underline{H}' = \underline{C}^\dagger \underline{H} \underline{C} = \begin{bmatrix} \alpha_1 & \beta_{11} & \dots & \beta_{1n} & 0 \\ \beta_{11} & E_1 & \dots & 0 & \beta_{21} \\ \vdots & \vdots & & \vdots & \vdots \\ \beta_{1n} & 0 & \dots & E_n & \beta_{2n} \\ 0 & \beta_{21} & \dots & \beta_{2n} & \alpha_2 \end{bmatrix} \qquad (4)$$

where

$$\beta_{1i} = \beta_{M-N} C_{2,i+1} \qquad \beta_{2i} = \beta_{M-N} C_{n+1,i+1} \qquad (5)$$

distribute the metal–nitogen interactions among all of the ligand orbitals. This ligand molecular orbital basis is a good choice of a basis for discussion of the properties of the metal–ligand interaction because the coupling matrix elements β_{1i} and β_{2i} are much smaller than typical differences between the diagonal matrix elements of $\mathbf{H}'$.

The spectral transition energies are the differences between the appropriate eigenvalues of $\mathbf{H}'$, plus additional terms. These additional terms include two-electron Coulomb and exchange energies, effects of configuration interaction, ligand polarizability, and most importantly, solvent shifts. We make no attempt to calculate these correction terms as they involve small differences between large quantities. Instead, we estimate them by introducing a simple empirical approximation. This is that every M → L state is shifted in energy by the same amount, and likewise for every L → M state. We identify (for a particular bridging ligand) the lowest energy M → L, L → M, and M → M (intervalence) transitions in the experimental spectra of the complexes with the energies $\Delta E_{L,II}$, $\Delta E_{III,H}$, and $\Delta E_{III,II}$, respectively. We use this information to determine the ligand HOMO–LUMO gap and the relative positions (α_1 and α_2 in eq 4) of the appropriate-valence Ru d_π orbitals within this band gap. Since we are concerned here only with relative energies, the modification to the Hamiltonian of eq 4 can be made in a number of ways. The simplest is the following: (1) set α for all Ru^{II} levels to zero, (2) set α for all Ru^{III} levels to $\Delta E_{III,II}$, (3) set the ligand LUMO level to $\Delta E_{L,II}$, adjusting all other ligand unoccupied orbital energies accordingly, and (4) set the ligand HOMO level to $\Delta E_{III,II} - \Delta E_{III,H}$, adjusting all other ligand occupied orbital energies accordingly. Note that the observed M → L, L → M, and M → M transition energies are given by the *eigenvalues* of $\mathbf{H}'$ rather than by the *matrix elements* controlled by $\Delta E_{L,II}$, $\Delta E_{III,H}$, and $\Delta E_{III,II}$, respectively; these quantities are closely related but are equal only in the case of zero metal–ligand coupling, i.e., $\beta_{M-N} = 0$. In any practical calculation, the energies $\Delta E_{L,II}$, and $\Delta E_{III,H}$, and $\Delta E_{III,II}$ are estimated, $\mathbf{H}'$ is diagonalized, and the transition energies are calculated. Adjustments of the parameters are then performed until the calculated transition energies match the observed values.

As an example, the structure of the energy matrix $\mathbf{H}'$ for the 4,4′-bipyridyl complexes is shown in Figure 2. The values of the empirical diagonal element differences $\Delta E_{L,II}$, $\Delta E_{III,II}$, and $\Delta E_{III,H}$, as well as the implied adjusted ligand HOMO–LUMO gap $\Delta E_{H,L}$, are indicated by vertical arrows. The adjusted HOMO–LUMO gap is clearly related to the first three energies by

$$\Delta E_{H,L} = \Delta E_{III,H} + \Delta E_{L,II} - \Delta E_{III,II} \qquad (6)$$

Thus, according to this very simple approach, the energies for all but the $\pi \rightarrow \pi^*$ transitions are calculated directly as differences between eigenvalues of the Hamiltonian $\mathbf{H}'$ parametrized in the above manner. A problem is that, for the $\pi \rightarrow \pi^*$ transitions, a further correction should be made to account for the large but compensating two-electron, solvation, and polarization terms. However, so as not to complicate the calculation we have chosen to quote uncorrected results for the $\pi \rightarrow \pi^*$ transitions. We note from Figure 2 that an effect of back-bonding is to destabilize the ligand LUMO level. As a result, the $\pi \rightarrow \pi^*$ frequency is higher in Ru^{II} complexes than in the corresponding Ru^{III} complexes.

The parameters in this model that are fitted to experiment are thus the metal–nitrogen coupling β_{M-N} (assumed constant throughout) and three experimental parameters per ligand specifying the relative positions of the ligand HOMO, LUMO, and d_π levels. The experimental param-

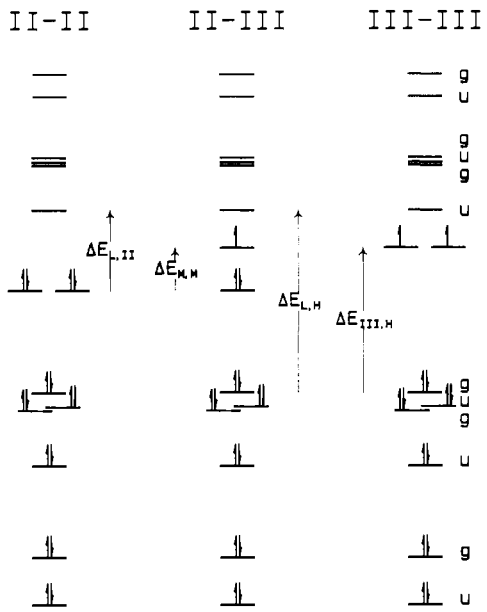

Figure 2. Uncoupled ($\beta_{M-N} = 0$) energy level diagram for the Ru^{II}–Ru^{II}, Ru^{II}–Ru^{III}, and Ru^{III}–Ru^{III} valence states of the $n = 0$ complex. The symmetries of the ligand orbitals with respect to the center of inversion are indicated by g and u.

Table I. Model Parameters[a]

ligand	r_{MM}/Å	energy gap/eV		
		$\Delta E_{III,II}$	$\Delta E_{L,II}$	$\Delta E_{III,H}$
pyridyl		2.41	2.99	4.33
$n = 0$	11.2	1.23	2.31	4.17
$n = 1$	13.4	1.34	2.23	3.33
$n = 2$	15.7	1.41	2.27	3.02
$n = 3$	18.0	(1.44)	(2.27)	(2.72)
$n = 4$	20.3	(1.45)	(2.27)	(2.50)

[a] For each ligand, the intermetallic distance r_{MM} is given as well as the Hamiltonian energy-gap parameters $\Delta E_{III,II}$, $\Delta E_{L,II}$, and $\Delta E_{III,H}$ deduced from experiment and, in parentheses, extrapolated from the $n = 2$ results.

eters, which are discussed further below, are listed in Table I for the pyridyl and the $n = 0$–2 ligands. This permits calculation of transition energies, intensities, and polarizations in all three states of ionization of the bis(metal) complexes. For the $n = 2$ bridge, for example, 15 transitions are so predicted in the accessible energy range. For the pyridyl complexes, no intervalence transition is possible and so no spectroscopic information is available for the energy difference between the Ru^{II} and Ru^{III} d_π levels. We set the splitting parameter $\Delta E_{III,II}$ in this case only in order to fit the observed $\pi \rightarrow \pi^*$ transition energies, using eq 6.

We note that while an intended use of this model is to verify the interpretation of the experimental spectra, the model is parametrized by data that are in turn drawn from the spectral interpretation. Thus, what results is a self-consistent solution to both problems rather than two independent solutions.

The Ru^{III}–Ru^{III} complexes are interesting in that they have two d_π orbitals occupied by just two electrons. Long-distance metal–metal coupling separates the symmetry-adapted linear combinations of the d_π orbitals by 400–800 cm^{-1} favoring a singlet ground-state S_0, while spin–orbit coupling (estimated at about 1000 cm^{-1} for a free Ru^{III} ion[27]) favors the triplet. Which state dominates at what temperature is a difficult theoretical problem,[28] outside the scope of this paper. Large differences in the electronic spectra are predicted, however, depending upon the identity of the dominant spin state (see Figure 3). From a singlet ground state, the lowest energy L → M transition is polarized in-plane but perpendicular to the Ru–N bond. As the polarization is perpendicular to the electronic motion, this absorption is expected to be rather weak. The second transition comes from a ligand orbital that has no coefficient on the nitrogen atoms, and thus, it also is weak. Like the first transition, the third transition is perpendicularly polarized, and it is not till the fourth transition that a strong L → M absorption arises. From a triplet

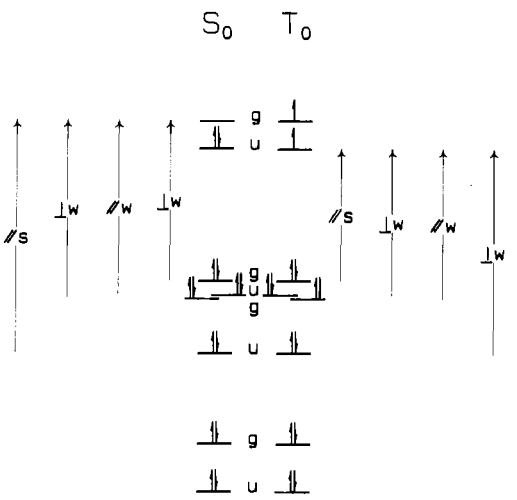

Figure 3. Electronic configurations and electronic excitations for the singlet S_0 and triplet T_0 ground states of Ru^{III}–4,4′-bipyridyl–Ru^{III}. Transitions are polarized in-plane and approximately either parallel (∥) or perpendicular (⊥) to the Ru–N bond vectors. Relative strengths are denoted by w (weak) and s (strong). All of the shown singlet excitations are allowed for the triplet state as well.

ground state, all of the above transitions are available plus some additional transitions. Its lowest lying L → M transition is polarized parallel to the Ru–N bond and is expected to be strong, with a series of weaker transitions following. All of the experimental L → M spectra show one strong band with weaker bands appearing at higher energy and are clearly spectra of a triplet ground state. This result is assumed in the following sections, and all calculated spectra shown correspond to excitation from the triplet state.

All of the electronic structure calculations are performed at a consistent series of molecular geometries in which all sp^2 bond angles are 120° and the bond lengths are $r_{C-C} = 1.36$ Å, $r_{C-C} = 1.45$ Å, $r_{C-C} = r_{C-N} = 1.39$ Å, and $r_{Ru-N} = 2.1$ Å. The results are not sensitive to physically realistic changes in the model geometries. Values for the intermetallic separation r_{MM} obtained from these model geometries are given in Table I for the bipyridyl complexes with $n = 0$–4.

The ligand SCF calculations are carried out both by the CNDO/S–CI method of ref 29 (this uses Mataga integrals) and, for some shorter molecules, by an ab initio calculation using a double-ζ basis set (for C and N we use a Roos and Siegbahn (7s,3p) basis set contracted to [4s,2p],[30] and for H we use a van Duijneveldt (3s) basis set contracted to [2s][31]). Our primary calculation technique is CNDO, and except where otherwise noted, all results reported in this paper are obtained by using it. The purpose of performing some ab initio calculations is to perform checks on the accuracy of the CNDO molecular orbitals and to make some estimation of the reliability of this part of the calculation method. In general, no significant differences are observed between results obtained with CNDO or ab initio techniques, though the calculated transition moments of the weak bands are usually less when ab initio rather than CNDO calculations are used.

Note that our approach uses the simplest possible model for the metal–nitrogen interaction and does not distinguish between different metal valence states, different ligands, or different geometries. Although it would be more realistic to distinguish between values of β_{M-N} for different oxidation states, the extra complexity necessary seems not warranted given the other assumptions involved and the difficulty in interpreting the experimental data. For the calculations using CNDO to determine the ligand orbitals, the value of β_{M-N} that gives the best overall fit to experiment is $\beta_{M-N} = -0.95$ eV. For the calculations that used the double-ζ basis set, a value of β_{M-N} must be specified between the Ru d_π orbital and both of the nitrogen π orbitals; we use −0.58 and −0.70 eV for coupling to the inner and outer nitrogen functions, respectively.

III. Fitting Spectra

The observed $\pi \rightarrow \pi^*$ and lowest lying M → L bands are fitted by using skewed Gaussian band contours, the exponents of which

(27) Hush, N. S.; Edgar, A.; Beattie, J. K. *Chem. Phys. Lett.* **1980**, *69*, 128.
(28) Girerd, J.; Jourhaux, Y.; Khan, O. *Chem. Phys. Lett.* **1981**, *82*, 534.
(29) Del Bene, J.; Jaffé, H. H. *J. Chem. Phys.* **1968**, *48*, 1807, 4050.
(30) Roos, B.; Siegbahn, P. *Theor. Chim. Acta* **1970**, *17*, 209.
(31) van Duijneveldt, F. B. Technical Report No. RJ-945; IBM: Armonk, NY, 1971.
(32) Navon, G.; Sutin, N. *Inorg. Chem.* **1974**, *13*, 2159.
(33) Waysbort, D.; Evenor, M.; Navon, G. *Inorg. Chem.* **1975**, *14*, 514.

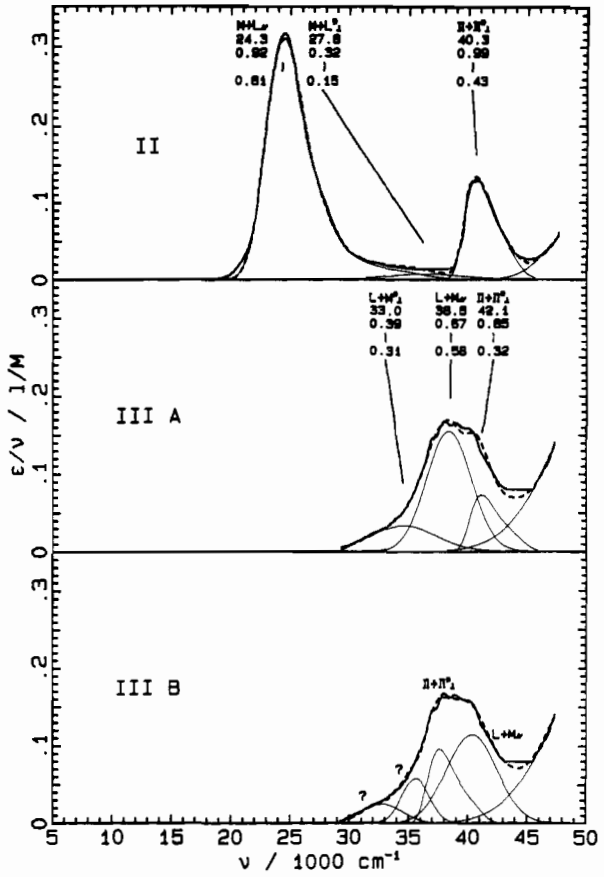

Figure 4. Interpretation of the observed spectra[13] of the pyridyl complexes. The dashed curves are the sum of the fitted curves (solid lines) and lie very close to the observed curves (uppermost solid lines). Theoretical calculations are marked near the observed bands and come in vertical blocks of five: top, the transition assignment and polarization in the molecular plane with respect to the Ru–N bond vector; second, the calculated band center in 10^3 cm^{-1}; third, the theoretical transition moment in e Å; fourth, a bar representing graphically the theoretical band center; bottom, the transition moment in e Å of the observed band.

Table II. Center ν_m, Fwhm Δ, Height $(\epsilon/\nu)_m$, and Transition Moment μ of the Deconvoluted $\pi \rightarrow \pi^*$ Bands

		valence state		
param	ligand	II or II–II	II–III	III or III–III
$\nu_m/10^3$ cm^{-1}	pyridyl	40.7		41.1
	$n = 0$	40.0	39.5	37.9
	$n = 1$	34.0	31.6	30.5
	$n = 2$	30.9	29.3	28.7
$\Delta/10^3$ cm^{-1}	pyridyl	3.1		3.1
	$n = 0$	6.8	6.8	6.8
	$n = 1$	6.9	6.9	6.9
	$n = 2$	4.9	4.9	4.9
$(\epsilon/\nu)_m/(L/M)$	pyridyl	0.13		0.07
	$n = 0$	0.39	0.25	0.21
	$n = 1$	0.58	0.59	0.86
	$n = 2$	0.99	1.34	1.70
μ/e Å	pyridyl	0.43		0.32
	$n = 0$	1.07	0.85	0.78
	$n = 1$	1.33	1.35	1.63
	$n = 2$	1.46	1.70	1.91

contain terms in powers of $(\nu - \nu_m)$ up to fourth order, where ν_m is the band center. All other bands are fitted by using simple Gaussian band contours. By the central limit theorem of statistics, inhomogeneously broadened electronic transitions (such as those produced when there exists a large number of slightly displaced, weakly coupled oscillators) have a Gaussian distribution of μ^2, where μ is the transition dipole moment. Thus, a plot of ϵ/ν versus ν is expected to have a Gaussian shape while a plot of ϵ versus λ is not. Results of the fits to the observed ϵ/ν versus ν spectra are given in Figures 4–7 for the pyridyl and n = 0–2 ligands,

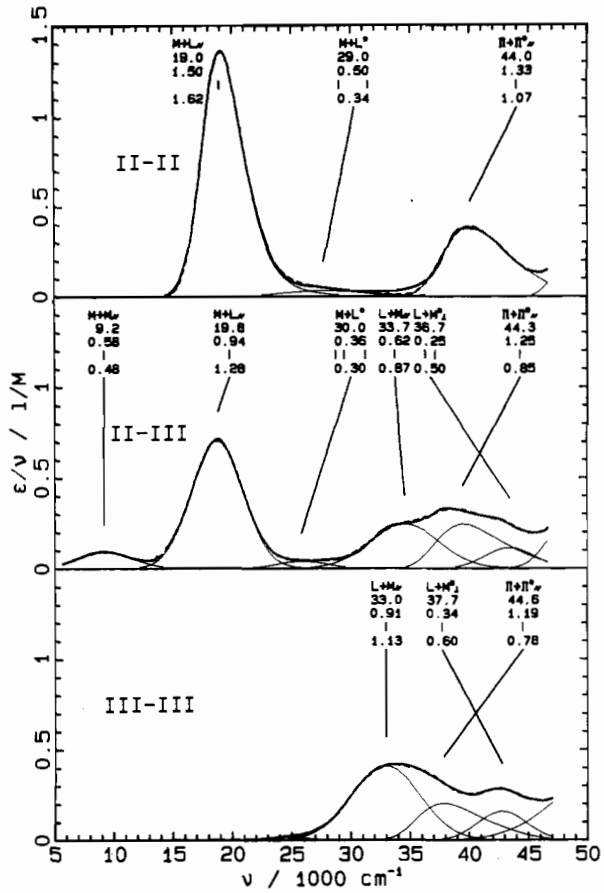

Figure 5. Interpretation of the observed spectra[14] of the $n = 0$ complexes. The hardly visible dashed curves are the sum of the fitted curves (solid lines) and lie very close to the observed curves (uppermost solid lines).

Table III. Center ν_m, Fwhm Δ, Height $(\epsilon/\nu)_m$, and Transition Moment μ of the Deconvoluted L → M and L → M* Bands

		valence state			
		II–III		III or III–III	
param	ligand	L → M	L → M*	L → M	L → M*
$\nu_m/10^3$ cm^{-1}	pyridyl			37.9	34.3
	$n = 0$	34.5	43.4	33.0	42.8
	$n = 1$	26.9	35.1	26.4	34.7
	$n = 2$	24.5	34.5	23.6	33.9
$\Delta/10^3$ cm^{-1}	pyridyl			4.4	6.2
	$n = 0$	6.8	4.8	6.8	4.8
	$n = 1$	3.3	5.0	3.3	5.0
	$n = 2$	4.1	6.3	4.1	6.3
$(\epsilon/\nu)_m/(L/M)$	pyridyl			0.16	0.03
	$n = 0$	0.25	0.12	0.41	0.41
	$n = 1$	0.17	0.16	0.35	0.35
	$n = 2$	0.37	0.34	0.57	0.57
μ/e Å	pyridyl			0.56	0.56
	$n = 0$	0.87	0.50	1.13	1.13
	$n = 1$	0.51	0.61	0.72	0.72
	$n = 2$	0.82	0.98	1.03	1.03

respectively, and the band centers ν_m, heights $(\epsilon/\nu)_m$, full widths at half-maximum Δ, and transition dipole moments μ are summarized in Tables II–V.

For all absorptions except the M → L transition, bands seen in more than one valence state are constrained to have the same band shape in each valence state, but the location and intensity of the band is allowed to vary. This enforces a degree of consistency upon the analysis but may not always be valid, particularly when the $\pi \rightarrow \pi^*$ excitation interacts strongly in one valence state but not in another. Relaxation of this constraint usually results in a minor reduction of the difference between the observed and fitted spectra but can result in major changes to bandwidths and intensities. Allowing only chemically reasonable changes to band shapes always results in fits that are qualitatively similar to the

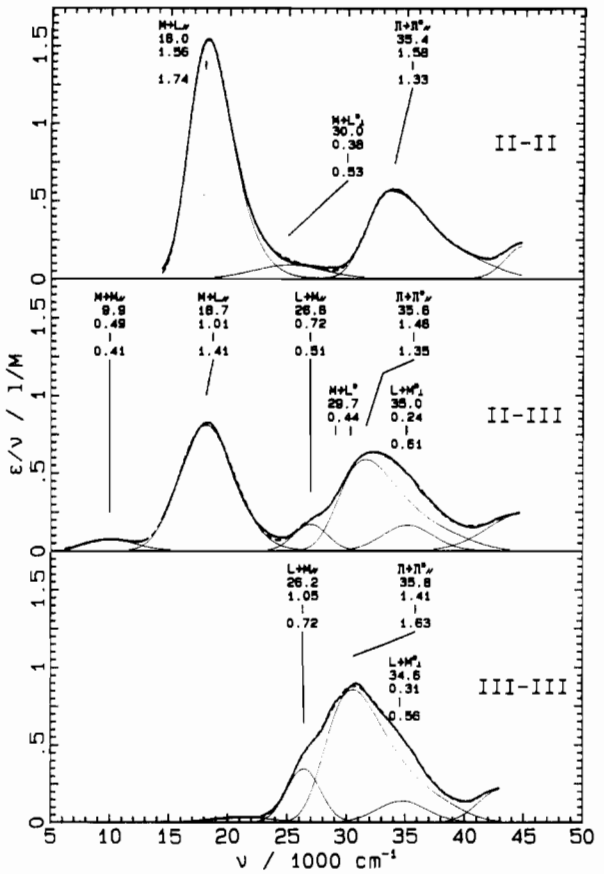

Figure 6. Interpretation of the observed spectra[14,25] of the $n = 1$ complexes. The hardly visible dashed curves are the sum of the fitted curves (solid lines) and lie very close to the observed curves (uppermost solid lines).

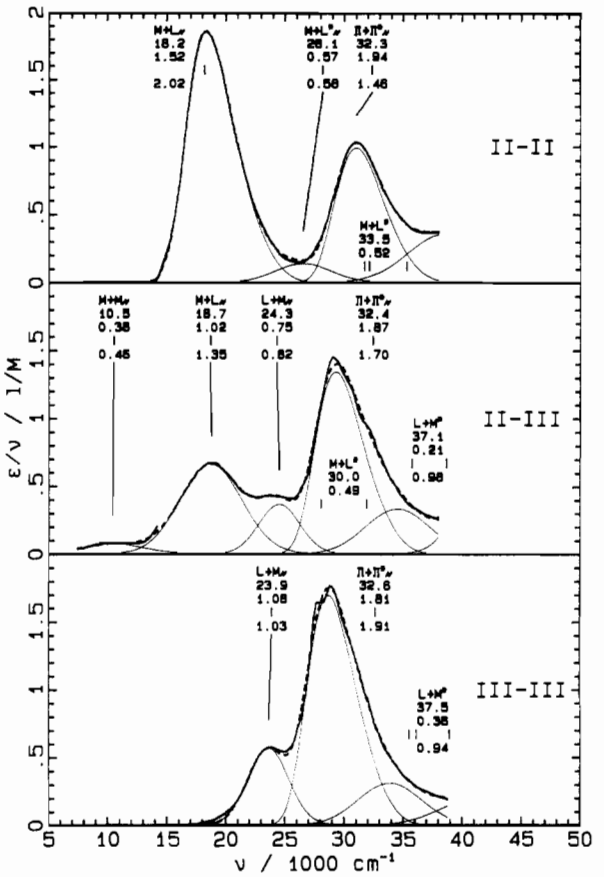

Figure 7. Interpretation of the observed spectra[15] of the $n = 2$ complexes. The hardly visible dashed curves are the sum of the fitted curves (solid lines) and lie very close to the observed curves (uppermost solid lines).

Table IV. Center ν_m, Fwhm Δ, Height $(\epsilon/\nu)_m$, and Transition Moment μ of the Deconvoluted M → L and M → L* Bands

		valence state			
		II or II–II		II–III	
param	ligand	M → L	M → L*	M → L	M → L*
$\nu_m/10^3$ cm^{-1}	pyridyl	24.4	35.8		
	$n = 0$	19.1	27.7	18.8	25.8
	$n = 1$	18.2	25.0	18.1	
	$n = 2$	18.3	26.5	18.7	
$\Delta/10^3$ cm^{-1}	pyridyl	4.4	7.2		
	$n = 0$	4.3	7.8	5.1	4.8
	$n = 1$	4.4	6.8	5.4	
	$n = 2$	5.1	5.4	6.0	
$(\epsilon/\nu)_m$/(L/M)	pyridyl	0.31	0.01		
	$n = 0$	1.36	0.03	0.71	0.30
	$n = 1$	1.54	0.09	0.81	
	$n = 2$	1.86	0.14	0.67	
μ/e Å	pyridyl	0.81	0.16		
	$n = 0$	1.63	0.34	1.28	0.04
	$n = 1$	1.74	0.53	1.41	
	$n = 2$	2.02	0.58	1.35	

ones reported here, but the weaker bands vary in dipole moment by as much as 0.2 e Å. Note that the M → L band is much broader in a mixed-valence ion than in a Ru^{II}–Ru^{II} ion because of the interaction with the intervalence M → M transition. Thus, this band is not constrained to have the same shape in both spectra.

The labels shown on Figures 4–7 show the theoretical results for, in order of decreasing height down the label, the following: (1) the band assignment and its polarization, (2) the calculated band center in 1000 cm^{-1}, (3) the theoretical transition dipole moment in e Å, (4) a line indicating graphically the band center, and (5) the fitted dipole moment of any spectral band identified with the theoretical prediction (in this case, either the label is placed next to the fitted band or a line is drawn connecting the label to the fitted band). As a variant to this format, if many

Table V. Center ν_m, Fwhm Δ, Height $(\epsilon/\nu)_m$, Transition Moment μ, and Effective Intermetallic Coupling $\bar{V}_{12}$ of the Deconvoluted M → M Bands

		valence state
param	ligand	II–III
$\nu_m/10^3$ cm^{-1}	$n = 0$	9.2
	$n = 1$	9.9
	$n = 2$ (A)	10.4
	$n = 2$ (B)	10.0
$\Delta/10^3$ cm^{-1}	$n = 0$	5.3
	$n = 1$	4.8
	$n = 2$ (A)	5.9
	$n = 2$ (B)	4.3
$(\epsilon/\nu)_m$/(L/M)	$n = 0$	0.093
	$n = 1$	0.076
	$n = 2$ (A)	0.076
	$n = 2$ (B)	0.061
μ/e Å	$n = 0$	0.48
	$n = 1$	0.41
	$n = 2$ (A)	0.46
	$n = 2$ (B)	0.34
$\bar{V}_{12}$/cm^{-1}	$n = 0$	390
	$n = 1$	300
	$n = 2$ (A)	305
	$n = 2$ (B)	215

weak L → M or M → L bands are predicted close together, then only one label is used in which part 2 is the average fequency, part 3 is the total dipole moment, and part 4 marks the positions of each of the individual bands.

Polarizations are indicated as being either parallel (∥) or perpendicular (⊥) depending upon the orientation of the transition dipole within the molecular plane to the Ru–N bond vectors. For the ligands with $n > 0$, this classification is, of course, only approximate. When many bands of different polarizations are grouped together, no polarization information is given in Figures 4–7.

Strong bands are labeled as either $\pi \rightarrow \pi^*$, L → M, or M → L, while weak bands tentatively are labeled L → M* or M → L*. Always, the assignments L → M and M → L refer to the dominant, intense, parallel-polarized transition of that particular type; all other transitions (including the lowest energy transition in pyridyl-Ru^{III} as well as transitions from the lower lying of the two metal d_π orbitals in II–II and III–III complexes) are labeled as either L → M* or M → L*, as appropriate. There is no definitive evidence for the assignments of the weak L → M* or M → L* bands; such assignments are made because theory predicts that a weak band should occur in the vicinity where a weak band is in fact observed. Both d → d transitions and impurities may also contribute to these weak absorptions.

In Table I the values of the energy-gap parameters $\Delta E_{III,H}$, $\Delta E_{L,II}$, and $\Delta E_{III,II}$ used in interpreting the pyridyl complex's and the n = 0–2 complexes' experimental spectra are given. A physically based interpretation for the changes observed in these quantities is given in Section V. The other parameter used in the calculations in Ru–N coupling is β_{M-N}, which is attributed a value of −0.95 eV throughout. This value is very similar to values deduced from simpler theories[12] for the ruthenium–nitrogen interaction in divalent and trivalent complexes with substituted pyridyl ligands.

a. Pyridyl Complex. In Figure 4 the observed and calculated spectra for the ruthenium(II) and ruthenium(III) pyridyl complexes are shown. The Ru^{II} spectrum shows a strong M → L band and a medium-strength $\pi \rightarrow \pi^*$ band (the pyridine ^1L_a band) joined by a shallow, flat absorption. A considerable overestimation of the $\pi \rightarrow \pi^*$ intensity is made, a result attributed to neglect of configuration interaction between the ligand HOMO → LUMO and HOMO − 1 → LUMO + 1 excitations. Overestimation of the $\pi \rightarrow \pi^*$ intensity is a feature present in almost all of our analyses, though to a much smaller extent as for the other ligands configuration interaction is not as important. The absorption between the strong bands is attributed to the first excited M → L* state, though this assignment is only tentative. Pyridine as a ligand is qualitatively different from the dipyridyl polyene ligands in that the $\pi \rightarrow \pi^*$ state is polarized perpendicular to the Ru–N bond vector. It thus interacts with the close-lying M → L* state, which may indeed give rise to the observed shallow absorption.

Two possible interpretations of the Ru^{III} spectrum are included as this spectrum is the most difficult to interpret of all those considered. In the n = 0–2 spectra, the $\pi \rightarrow \pi^*$ transition is seen to move to lower energy as the metal oxidation state increases, and the interpretation of the spectrum of the pyridyl complex consistent with this trend is labeled "B" in Figure 4. However, with this assumption, it is then rather difficult to fit the low-frequency tail of the absorption band, and two Gaussians are used for this purpose in Figure 4. Calculations show that, for this ligand only, the weak perpendicular-polarized transition L → M* is of lower energy than is the strong parallel-polarized L → M transition (note that, in our notation, the lowest parallel-polarized ligand to metal transition is always called L → M, while all other ligand to metal absorptions are called L → M*; in corresponding molecules, all transitions labeled L → M thus correspond to transitions of similar form). In this interpretation, the absorption to the blue of the $\pi \rightarrow \pi^*$ band would be attributed to the intense L → M transition, while part of the absorption to the red would be attributed to the weak L → M* transition. The additional part of the absorption to the red of $\pi \rightarrow \pi^*$ could be attributed to metal d → d transitions (observed in $Ru^{III}(NH_3)_6$[32,33] at ν_m = 36 000 cm^{-1}, $(\epsilon/\nu)_m$ = 0.013 L/M, and Δ = 7000 cm^{-1}) or to pyridine's ^1L_b transition.

Interpretation B is unlikely, however, because of the small energy spacing of ≈3000 cm^{-1} required between the $\pi \rightarrow \pi^*$ and L → M* bands. CNDO gives a coupling between these bands of 4200 cm^{-1} (as a check of this calculation, the result obtained using the double-ζ basis is almost identical at 4100 cm^{-1}). Configuration interaction reduces this coupling by only a small amount, to 3500 cm^{-1}. Consequently, the minimum separation permissible between the $\pi \rightarrow \pi^*$ and L → M* bands is about 7000 cm^{-1}, which is much more than the fitted separation. We thus reject this interpretation of the spectrum.

Labeled "A" is an alternative interpretation that places the $\pi \rightarrow \pi^*$ band at the high-frequency end of the observed band contour. Here it is ≈8500 cm^{-1} away from the L → M* band, and both bands are comparable in intensity. This suggests that the observed bands are the product of a near-resonant interaction between the original $\pi \rightarrow \pi^*$ and L → M* bands, with perhaps the higher frequency band being dominated slightly by the $\pi \rightarrow \pi^*$ transition. If so, then one would not expect the $\pi \rightarrow \pi^*$ band to have the same shape as in the Ru^{II} complex, and indeed allowing this band contour to relax does improve the fit but makes no significant qualitative difference. It is interpretation A that is recorded in Tables II–V.

b. 4,4′-Bipyridyl (n = 0) Complex. The observed and calculated spectra for the n = 0 complex are shown in Figure 5 for the Ru^{II}–Ru^{II}, Ru^{II}–Ru^{III}, and Ru^{III}–Ru^{III} valence species. Note that the Ru^{II}–Ru^{III} spectrum is corrected for comproportionation. Contrary to the situation with pyridyl complex, the $\pi \rightarrow \pi^*$ state for the n = 0 complex is polarized parallel to the Ru–N bond vector; thus it interacts with the low-lying M → L and L → M states rather than with the nearby M → L* and L → M* states. The ligand molecular orbitals of n = 0 are delocalized over twice the number of centers than they are for the pyridyl complex, and thus, the couplings β_{1i} and β_{2i} are significantly reduced. These changes considerably weaken the strong interactions seen in the pyridyl complex, and consequently the spectra are simplier to interpret.

For the Ru^{II}–Ru^{II} complex, the M → L and $\pi \rightarrow \pi^*$ transitions are clearly resolved with a shallow absorption (in the range 25 000–30 000 cm^{-1}) bridging them. This bridging absorption is tentatively assigned to a M → L* band, though alternative explanations are possible. Good agreement is seen between the calculated and observed intensity of this weak transition.

In the Ru^{II}–Ru^{III} complex, the M → L transition is much weaker. The intervalence M → M band is quite clearly resolved and highly Gaussian in shape, but note that the experimental spectra are incomplete because two different spectrometers, with nonoverlapping frequency ranges, were used in making the measurements. Interpolation between these two sets of results appears straightforward, however, affirming the quality of the experimental results. Three bands are resolvable in the 30 000–45 000-cm^{-1} region, and these are interpreted as the L → M band, a L → M* band, and the $\pi \rightarrow \pi^*$ band by comparison with the related bands in the Ru^{III}–Ru^{III} complex, as discussed below. Note that the $\pi \rightarrow \pi^*$ band is predicted to be 4000 cm^{-1} higher than the observed band: this is because explicit corrections for configuration interaction, two-electron Coulomb and repulsion energies, solvation energies, and polarization on the structure of the ligand orbitals are not included. In the intermediate region (25 000–3000 cm^{-1}) between the intense absorptions, a weak absorption is seen. It is attributed to three weak, strongly overlapping M → L* transitions of mixed polarization.

For the Ru^{III}–Ru^{III} complex, three distinct but overlapping bands are seen, and these bands are clearly related to bands seen in the spectrum of the Ru^{II}–Ru^{III} complex. Theory predicts that the lowest L → M transition should grow significantly in intensity in the Ru^{III}–Ru^{III} complex compared to that in the Ru^{II}–Ru^{III} complex. Similarly, a small decrease in the $\pi \rightarrow \pi^*$ intensity is predicted and a small decrease in the L → M* intensity is predicted. Hence, we conclude that the $\pi \rightarrow \pi^*$ band is located at the center of the observed absorption band with the L → M band at the low-frequency end.

A possible problem with this interpretation of the Ru^{II}–Ru^{III} and Ru^{II}–Ru^{III} spectra is that the calculated separation between the L → M and L → M* bands is 4700 cm^{-1} (as a check, double-ζ calculations give 5100 cm^{-1}) whereas the fitted splitting is much larger, 10 200 cm^{-1}. Because the L → M and L → M* transitions have different symmetries, it is conceivable that the calculations are in error (previously, for the pyridyl ligand, option B was rejected because the states in question possess the same symmetry, and thus, it is inconceivable that the calculations are seriously in error). However, excellent agreement for the L → M to L → M*

Table VI. Physical Interpretation of $\Delta E_{L,II}$ and $\Delta E_{III,H}$[a]

ligand	$\delta\Delta E_{L,II}$	δE_{LUMO}	$\delta\Delta E_{III,H}$	δE_{HOMO}
$n = 0$	−0.68	−0.87	−0.16	−0.34
$n = 1$	−0.76	−1.08	−1.00	−0.99
$n = 2$	−0.72	−1.22	−1.31	−1.42
$n = 3$		−1.31		−1.72
$n = 4$		−1.38		−1.94

[a] $\delta\Delta E_{L,II}$ and $\delta\Delta E_{III,H}$ are the changes in the parameters $\Delta E_{L,II}$ and $\Delta E_{III,H}$ (as given in Table I) from their respective values for the pyridyl complexes. They correspond to changes δE_{LUMO} and δE_{HOMO} in the ligand LUMO and HOMO orbital energies evaluated by using CNDO, respectively. All energies are in eV.

splitting is obtained for the $n = 1$ ligand, and thus one is suspicious of this $n = 0$ result.

A possible alternative analysis is that both the $\pi \rightarrow \pi^*$ band and the L → M band are resonant near 35 000–36 000 cm^{-1}, and because of the interaction between them (2700 cm^{-1} as calculated from both CNDO and double-ζ ligand descriptions), the two bands interact and move apart. Thus, the observed bands would be nearly equal mixtures of the $\pi \rightarrow \pi^*$ and L → M bands. The parameter $\Delta E_{III,H}$ for $n = 0$ in Table I should be about 0.3 eV higher in this case, giving much poorer agreement between theory and experiment in Table VI. Other evidence to support the alternative analysis comes from comparisons of the changes in $\pi \rightarrow \pi^*$ energy with valence state for different ligands. The first interpretation results in a steady decrease in the $\pi \rightarrow \pi^*$ frequency of 2100 cm^{-1} as one goes from Ru^{II}–Ru^{II} via Ru^{II}–Ru^{III} to Ru^{III}–Ru^{III}; this is of the correct sign but is smaller than the value naively expected by extrapolating the decreases of 3500 and 2100 cm^{-1} seen in the $n = 1$ and $n = 2$ spectra, respectively (see later). In the alternative analysis, the $\pi \rightarrow \pi^*$ and L → M interaction would result in a compression of the expected $\pi \rightarrow \pi^*$ energy change, as observed.

There is neither sufficient theoretical nor experimental evidence available to choose between these two interpretations of the spectra, and the more conservative first interpretation is presented in Figure 5 and in Tables II–VI.

c. $n = 1$ Complex. Spectra of this complex are qualitatively similar to those of the $n = 0$ complex. Compared to those of the $n = 0$ spectra, the $\pi \rightarrow \pi^*$ band grows significantly in intensity while the M → L and L → M bands grow only slightly; both the L → M and the $\pi \rightarrow \pi^*$ band move to considerably lower frequency. Because of the increased $\pi \rightarrow \pi^*$ strength, there exists no ambiguity as to the location of this band with respect to the L → M and L → M* bands. The M → L band in the Ru^{II}–Ru^{III} species is again much broader than the M → L band in the Ru^{II}–Ru^{II} species, and the intervalence M → M band is well resolved and highly Gaussian in contour.

d. $n = 2$ Complex. For the $n = 0$ and $n = 1$ complexes, Taube et al. measured the comproportionation constant K_c

$$Ru^{II}\text{–}Ru^{II} + Ru^{III}\text{–}Ru^{III} \overset{K_c}{\rightleftharpoons} 2Ru^{II}\text{–}Ru^{III} \qquad (7)$$

and used this to deduce the spectra of the Ru^{II}–Ru^{III} ions from a knowledge of the spectra of equilibrium distributions of Ru^{II}–Ru^{III}, Ru^{II}–Ru^{II}, and Ru^{III}–Ru^{III} ions as well as the spectra of the individual Ru^{II}–Ru^{II} and Ru^{III}–Ru^{III} ions. As K_c becomes smaller, it becomes increasingly more difficult to measure, and so Woitellier, Launay, and Spangler[15] did not measure K_c, choosing to report just the spectrum of the equilibrium mixture. It is possible to estimate K_c by using a simple theory that sees K_c as deviating from the entropic factor of 4 by an amount related to the Coulomb repulsion energy of the metal charges. Coulomb's law gives

$$\Delta H = \Delta U = -(\epsilon r_{MM})^{-1} \qquad (8)$$

where ϵ is the dielectric constant of the material between the metal atoms separated a distance r_{MM}, so that K_c is given by

$$K_c = 4 \exp\left(\frac{1}{\epsilon r_{MM} kT}\right) \qquad (9)$$

Using the intermetallic separations given in Table I and Sutton and Taube's observed value[10] of $K_c = 20$ for $n = 0$, we conclude that $\epsilon = 31$. Applying eq 9 for the $n = 1$ case then gives $K_c = 15.4$, close enough to the value measured by Sutton and Taube of $K_c \approx 14$ to suggest that this crude theory is reliable enough for the purpose. We thus predict the value $K_c = 12.7$ for the $n = 2$ case and use this value to extract the spectrum of the Ru^{II}–Ru^{III} complex from the spectra given by Woitellier, Launay, and Spangler; the result is shown in Figure 7.

The trends seen in going from $n = 0$ to $n = 1$ are continued in going from $n = 1$ to $n = 2$. Because of the compression in the frequency scale, all traces of the weak absorptions that previously were attributed to M → L* transitions are lost. One difficulty in the interpretation of the experimental spectra arises because the infrared and visible spectra taken by Woitellier, Launay, and Spangler[15] appear not to connect smoothly. Another absorption band may be present between the M → M and M → L bands, but this is unlikely because no trace of such a band exists in the spectra of the other ligands. Rather, one or both of the spectrometers may not have given accurate results at the limits of their observation windows, or problems arising from the poor solubility of the $n = 2$ complexes in D_2O may have given rise to erroneous extinction scales. The interpretation presented in Figure 7 assumes that the infrared spectrum is incorrect at its high-frequency end; this result is labeled A in Table V and gives the transition moment $\mu = 0.46$ e Å. An alternative interpretation is possible on the basis of the assumption that the visible spectrum is correct but that the infrared spectrum is poorly scaled. This is likely because the trends seen in the $\pi \rightarrow \pi^*$ and M → L band intensities are quite plausible, while the infrared spectrum is much more difficult to obtain. This interpretation is labeled B in Table V and gives $\mu = 0.34$ e Å. It produces a much more consistent set of changes in the M → M band as a function of n. Assuming that the infrared band is correct but the visible band is improperly scaled gives a transition moment of $\mu = 0.39$ e Å, while ignoring the visible spectrum altogether and fitting just the infrared spectrum gives $\mu = 0.45$ e Å. The theoretical calculations overestimate the transition moment of the $n = 0$ and $n = 1$ species by about 20% so that one would expect a similar overestimation in the $n = 2$ case giving an expected observed $\mu \approx 0.32$ e Å, in agreement with interpretation B only. A large uncertainty thus exists in the value of the observed intervalence dipole moment, and we conclude that $\mu = 0.39 \pm 0.07$ e Å.

IV. Interpretation of Changes in $\Delta E_{III,H}$, $\Delta E_{L,II}$, and $\Delta E_{III,II}$

It is possible to interpret the changes in $\Delta E_{L,II}$ and $\Delta E_{III,H}$ shown in Table I from theoretical considerations. In this fashion, these parameters are seen to describe real physical properties of the complexes that are thus transferable to other systems, rather than being just fitting parameters (as is the case when Hückel models are used[26]).

In Table VI, the changes δE_{LUMO} and δE_{HOMO} calculated by using CNDO in the ligand LUMO and HOMO energies from the LUMO and HOMO energies of pyridine are given. As the size of the ligand increases, the LUMO energy of the ligand falls slightly and the energy of the HOMO level increases appreciably. Assuming that the metal d_π levels stay at the same energy and that solvation polarization, Coulomb, and exchange energies do not change appreciably, then these changes in the LUMO and HOMO energies should result in a lowering of the energy gaps $\Delta E_{L,II}$ and $\Delta E_{III,H}$. For comparison, the changes $\delta\Delta E_{L,II}$ and $\delta\Delta E_{III,H}$ seen in Table I of $\Delta E_{L,II}$ and $\Delta E_{III,H}$ for the dipyridyl polyene complexes from the respective values for the pyridyl complexes are also given in Table VI. The changes in the L → M energy parameter $\Delta E_{III,H}$ closely parallel the HOMO energy changes, although the comparison of the changes in the M → L energy parameter $\Delta E_{L,II}$ to the LUMO level changes is not as good. An additional effect is seen that *raises* $\Delta E_{L,II}$ by about 0.15 eV for each transition as the ligand is changed pyridyl → $n = 0$ → $n = 1$ → $n = 2$. Certainly, the major changes seen in the parameters $\Delta E_{L,II}$ and $\Delta E_{III,H}$ are attributable to changes in the ligand orbital energies.

V. Calculations for $n = 3$ and $n = 4$ Complexes

Woitellier, Launay, and Spangler,[15] have synthesized the next members $n = 3$ and $n = 4$ of the all-trans 4,4′-bipyridyl polyene series but, because of solubility problems in D_2O, were forced to record only limited spectra taken in nitrobenzene. Thus, experimental data are not available for the determination of the parameters $\Delta E_{III,H}$, $\Delta E_{L,II}$, and $\Delta E_{III,II}$. With the hope that one day measurements for these complexes in D_2O will be possible, later we make predictions of their electronic couplings by using estimates of $\Delta E_{III,H}$, $\Delta E_{L,II}$, and $\Delta E_{III,II}$. We estimate these parameters by extrapolating the $n = 2$ results, applying the trends shown in the $n = 0$–2 data in Table I in conjunction with the CNDO results for the changes in the ligand LUMO and HOMO levels shown in Table VI. These extrapolated values are shown in parentheses in Table I, and all results obtained on the basis of these numbers are also shown in parentheses in subsequent tables.

An interesting situation is expected for these complexes, as $\Delta E_{L,II}$ appears steady at ≈2.3 eV while $\Delta E_{III,H}$ decreases toward $\Delta E_{L,II}$. The spectra for the mixed-valence Ru^{II}–Ru^{III} analogues of $n = 3$ and $n = 4$ may thus be difficult to interpret, as the L → M and M → L transitions may overlap and, more importantly, the tail of L → M bands may interfere with the intervalence M → M absorption.

VI. Intermetallic Coupling

It is the usual practice to describe the intermetallic coupling by using an effective two-level model. This assumes that the observable effects resulting from the long-distance through-bridge-modulated interaction are the same as the observable effects resulting from the situation in which the two metal orbitals interact directly through-space with a coupling matrix element $\bar{V}_{12}$. If this coupling is small (as indeed it must be in order that an effective two-state model is appropriate[34]), then perturbation theory allows $\bar{V}_{12}$ to be deduced[1] from the parameters of the deconvoluted intervalence band:

$$\bar{V}_{12} = \mu\nu_m/r_{MM} \tag{10}$$

where μ is in units of electron angstroms and r_{MM} in angstroms is the intermetallic separation. From the results in Tables I and V, we deduce the couplings $\bar{V}_{12}$ given in Table V. The values for $n = 0$ and $n = 1$ are very close to the results published originally by Taube et al.,[14] and one estimates that these numbers are accurate to about ±15 cm^{-1}. Because of the ambiguities in the interpretation of the M → M spectrum for $n = 2$ discussed earlier, the possible values of $\bar{V}_{12}(2)$ range from 215 to 305 cm^{-1}. Thus, we conclude that $\bar{V}_{12}(2) = 260 \pm 45$ cm^{-1}. From McConnell's theory,[35] one expects that the coupling should decrease exponentially as n increases according to

$$\bar{V}_{12}(n) = \bar{V}_{12}(0)e^{-\gamma n} \tag{11}$$

An exponential extrapolation of the $n = 0$ and $n = 1$ results predicts that $\bar{V}_{12}(2) = 230$ cm^{-1}, which is inside the experimental range, so we see that in order to test theories (e.g. refs 34 and 36) for nonexponential bridge-length dependences, experimental data must be of the highest quality.

A difficulty in the interpretation of this experimental data arises from the relatively low barriers to planarity breaking torsional motions. For 4,4′-bipyridine, the torsional potential about the inter-ring bond is known from NMR data[37] to have a minimum at 37°. We performed some calculations for the $n = 0$ complex at twisted geometries and found only minor changes resulted to the calculated band intensities and positions for all bands except the intervalence M → M band. For this band, μ decreased approximately with the cosine of the torsional angle. From the known[37] torsional potential $V(\theta)$, the expectation value at room temperature of the cosine of the angle may be evaluated, leading to a definition of the coupling-weighted thermally averaged angle as

$$\bar{\theta} = \arccos\left[Z^{-1}\int_0^{\pi/2}\cos\theta\, e^{-V(\theta)/kT}\, d\theta\right] \tag{12}$$

where Z is the canonical partition function

$$Z = \int_0^{\pi/2} e^{-V(\theta)/kT}\, d\theta \tag{13}$$

This evaluates to $\bar{\theta} = 32°$ for 4,4′-bipyridine.

Evidence to suggest the validity of the cosine law is discussed in detail by Woitellier, Launay, and Joachim,[38] who performed extensive extended Hückel calculations for the $n = 0$ complex. Corroborative experimental evidence comes from the study of the $n = 0$ complex substituted adjacent to the interring bond to produce complexes with large equilibrium torsional displacements. The effective intermetallic coupling in bis(pentaammineruthenium) 2,6-dimethyl-4,4′-bipyridine is known[10] to be 195 cm^{-1}, which, given the above results for $n = 0$ and the cosine relationship, predicts that the torsional angle in the dimethyl complex is 65°. This number is not known from direct observation, but Field and Sternhell[39] using NMR spectroscopy showed that the equilibrium torsional angles for 2,6-dichloro-4,4′-bipyridyl and for 2,6-dibromo-4,4′-bipyridyl in solution are 68 and 69°, respectively. As these halogen substituents have steric bulk comparable to that of the methyl substituents, one would expect a similar (if not slightly smaller) torsional angle, implying the appropriateness of the cosine law.

For the analogous torsional motions in the polyene-bridged ligands, styrene is a suitable model compound. In the gas phase, styrene is known from microwave studies[40] to be planar but with a very shallow potential. The coupling-weighted thermally averaged angle from eq 12 is $\bar{\theta} = 17°$. We performed calculations for the $n = 1$ and $n = 2$ ligands using conformations rotated about each pyridyl–polyene bond by ±17° and found again that only the transition moments for the M → M transitions are significantly affected. To a good approximation, the cosine law per angle appeared to describe the coupling adequately.

Complexes with $n > 1$ may also undergo torsional motions, which destroy the planarity of the C=C—C=C units. These torsions are expected to be smaller in amplitude than the torsions involving the rings, and thus we do not treat them explicitly. The number of such torsions increases as the chain-length n increases, however, and the observed coupling for complexes such as $n = 4$ could be significantly decreased because of these torsional modes.

For the purpose of developing theories of long-range electron-transfer processes, it is important at this time to perform experiments that measure only the electronic couplings. The nature of the length dependence of this coupling is of primary fundamental importance; details of the geometries, etc., are seen to be specific to particular applications and thus of secondary importance. It is desirable to perform experiments on rigid molecular systems, to which the dipyridyl polyenes form a useful

Table VII. Effective Intermetallic Coupling Constant (cm^{-1}) for Hypothetical Planar Pentaammineruthenium Complexes in 0.1 M DCl/D_2O

	photoinduced		thermal $\bar{V}_{12}^{(R)}$		
ligand	obs	calc	$\sigma = 0$	$\sigma = 0.1/2^{1/2}$	$\bar{V}_{12}^{(J)}$
$n = 0$	460	476	214	395	443
$n = 1$	330	364	138	282	312
$n = 2$	285 ± 50	253	82	190	202
$n = 3$		(185)	(52)	(134)	(137)
$n = 4$		(136)	(33)	(92)	(92)

(34) Reimers, J. R.; Hush, N. S. *Chem. Phys.* **1989**, *134*, 323.
(35) McConnell, H. M. *J. Chem. Phys.* **1961**, *35*, 508.
(36) Joachim, C. *Chem. Phys.* **1987**, *116*, 339.
(37) Emsley, J. W.; Stephenson, D. S.; Lindon, J. C.; Lunazzi, L.; Pulga, S. *J. Chem. Soc., Perkin Trans. 1* **1975**, 1541.
(38) Woitellier, S.; Launay, J. P.; Joachim, C. *Chem. Phys.* **1989**, *131*, 481.
(39) Field, L. D.; Sternhell, S. *J. Am. Chem. Soc.* **1981**, *103*, 738.
(40) Caminati, W.; Vogelsanger, B.; Bauder, A. *J. Mol. Spectrosc.* **1988**, *128*, 384.

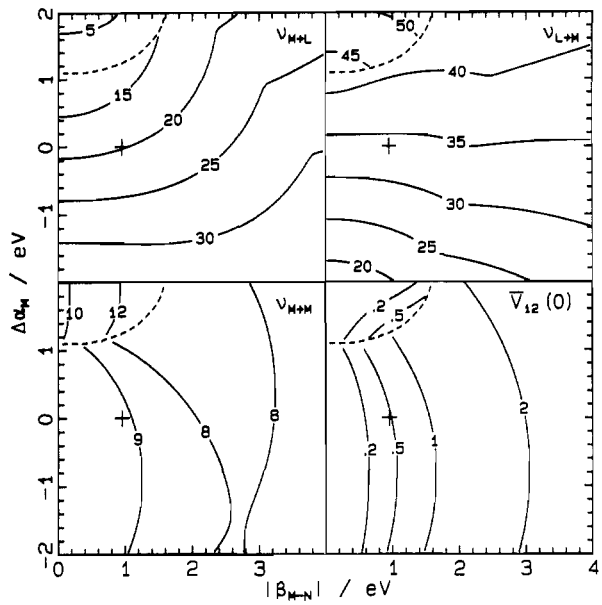

Figure 8. Contours in 10^3 cm^{-1} for the $n = 0$ complex of the M → L, L → M, and intervalence M → M transition energies and the effective intermetallic coupling constant $\bar{V}_{12}$ as functions of the metal to nitrogen interaction strength β_{M-N} and the change in energy of the metal d_π levels from the bis(pentaammineruthenium) complexes $\Delta\alpha_M$ (eq 16). The reorganization energy $\Delta E_{III,II}$ is fixed at 1.23 eV, and the plus sign indicates the point appropriate for the bis(pentaammineruthenium) complexes. Marked by a dashed line is the discontinuity causes by the crossing of the M → L and M → M states: this is approximately the $\nu_{M\to L}$ = 10000 cm^{-1} contour line.

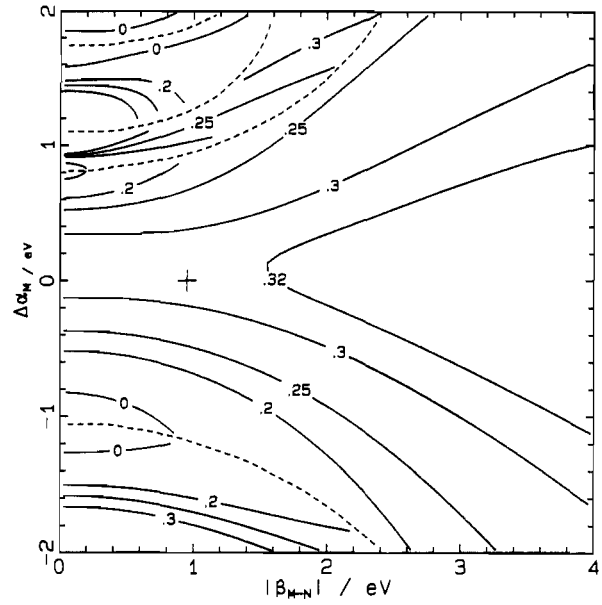

Figure 9. Contours of the average bridge-length dependence γ evaluated over $n = 0$–4 for photoinduced electron transfer as functions of the metal to nitrogen interaction strength β_{M-N} and the change in the d_π energies $\Delta\alpha_M$ (eq 16). All contours with γ = 0, 0.2, 0.25, and 0.3 are shown, as well as one contour with γ = 0.32. Discontinuities in γ caused by resonances are marked by dashed lines.

approximation. By assumption of the validity of the cosine relationships, nonplanarity corrections may be introduced to the experimental coupling constants, giving corrected experimental couplings $\bar{V}_{12}$ for hypothetical planar ligands. Corrected couplings are given in Table VII; the related multiplicative correction factors used are $\cos^{-1} 32° = 1.206$ for $n = 0$, and $\cos^{-2} 17° = 1.093$ for $n = 1$ and $n = 2$. Inclusion of a C=C—C=C correction term for $n = 2$ would increases this value by a small amount.

It is also possible to calculate $\bar{V}_{12}$ by using in eq 10 the theoretical predictions of μ and ν_m, and the results are given in Table VII. Here, predictions are made not only for the $n = 0$–2 complexes but also for the $n = 3$ and 4 complexes on the basis of the parameters extrapolated in section V from the $n = 2$ parameters. Good agreement is seen between these theoretical values and the angle-corrected experimental values, though it is desirable to improve the accuracy of the experimental result for $n = 2$ because some of the possible interpretations of the spectra are consistent with the theoretical result while others are not.

The falloff of the coupling seen in the theoretical results is quite close to exponential falloff. A measure of the degree of nonexponentiality (appropriate only in the monotonic regimes[21,22,41]) is the ratio of the slopes of the decay curve at its extremities defined as

$$\zeta = \frac{\bar{V}_{12}(1)\bar{V}_{12}(3)}{\bar{V}_{12}(0)\bar{V}_{12}(4)} \qquad (14)$$

From the results given in Table VII, theory predicts $\zeta = 0.96$, quite close to the value of unity expected for exponential decay. This small amount of nonexponential behavior results from the closeness of the Ru^{III} d_π orbital to the ligand virtual orbitals; see Figure 2. Because the deviation from exponentiality is only small, we define as a measure of the coupling an average falloff γ evaluated over the range $n = 0$–4 as

$$\gamma = \tfrac{1}{4} \log \frac{\bar{V}_{12}(4)}{\bar{V}_{12}(0)} \qquad (15)$$

This evaluates to give an average bridge-length dependence of $\gamma = 0.31$ from the theoretical data given in Table VII.

VII. Effects of Substitution

It is possible to synthesize a wide range of complexes like the α,ω-dipyridyl polyenes, which display long-range electron transfer by substitution in the pyridyl ring, in the inner coordination shell, and by substituting the metal itself. Complexes that display high intermetallic coupling with less than exponential bridge-length dependences are sought as they have both scientific and commercial significance, and by adaptating the parameters in the theoretical model, we predict which substitutions are most likely to lead to highly coupled complexes. Basically, this requires that the d_π levels of the complex are taken close to resonance with the orbitals of the ligand and, in the context of our model Hamiltonian, can arise due to modifications of either $\Delta E_{L,II}$, $\Delta E_{III,H}$, or $\Delta E_{III,II}$. Decreasing $\Delta E_{L,II}$ and increasing $\Delta E_{III,II}$ forces the Ru^{III} orbital toward the ligand LUMO orbital, see Figure 2, while decreasing $\Delta E_{III,H}$ forces the Ru^{II} level toward the ligand HOMO level. As the Ru^{III} level is much closer to the LUMO level than the Ru^{II} level is to the HOMO level, it is recommended to search for substitutions that raise the metal d_π orbital energies.

Let X be an arbitrary metal–ligand complex. We assume that the solvent reorganization energy $\Delta E_{III,II}$ is not significantly affected by substitution and plot in Figure 8 contours of the band maxima $\nu_{M\to L}$, $\nu_{L\to M}$, and $\nu_{M\to M}$, versus both the metal to nitrogen coupling β_{M-N} and the change $\Delta\alpha_M$ in the d_π orbital energies of X from the bis(pentaammineruthenium) α,ω-dipyridyl polyene complexes (BPRuBP); i.e.

$$\Delta E_{III,II}(X) = \Delta E_{III,II}(BPRuBP)$$
$$\Delta E_{III,H}(X) = \Delta E_{III,H}(BPRuBP) + \Delta\alpha_M \qquad (16)$$

and

$$\Delta E_{L,II}(X) = \Delta E_{L,II}(BPRuBP) - \Delta\alpha_M$$

so that

$$\Delta E_{H,L}(X) = \Delta E_{H,L}(BRPuBP) \qquad (17)$$

Contours of the effective coupling $\bar{V}_{12}(0)$ are also given in Figure 8, and contours of the average bridge-length dependence γ (see eq 14) and the nonexponentiality ζ (see eq 10) are given in Figures 9 and 10, respectively. In each of these figures, the point cor-

(41) Reimers, J. R.; Hush, N. S. *Chem. Phys.*, in press.

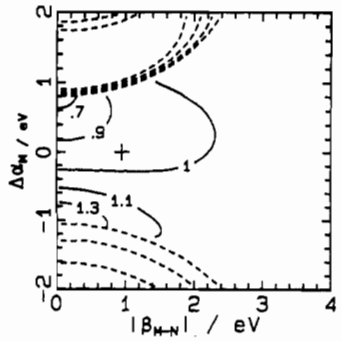

Figure 10. Contours of the exponentiality parameter ζ evaluated over $n = 0$–4 for photoinduced electron transfer as functions of the metal to nitrogen interaction strength β_{M-N} and the change in the d_π energies $\Delta\alpha_M$ (eq 16). Discontinuities in ζ caused by resonances are marked by dashed lines, and for simplicity, the contours are only drawn within the central region.

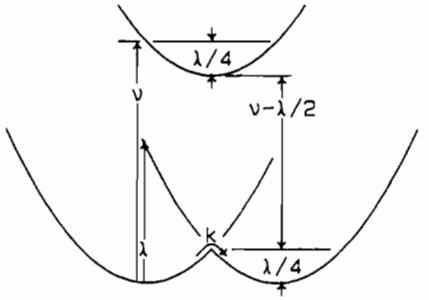

Figure 11. Potential energy surfaces for photoinduced and thermal electron transfer. Photoinduced transfer involves a Condon absorption of energy $\lambda = \Delta E_{III,II}$ whereas thermal transfer involves a rate constant k for barrier crossing. Here, $\nu \approx \Delta E_{L,II}$ or $\Delta E_{III,H}$ is the absorption frequency of the ligand charge hole transfer states. The reorganization energy is λ.

Table VIII. II/III Reduction Potentials (V) for Various Complexes versus NHE[a]

isomer	metal	ligand set	E_0	ref
	Os	$(NH_3)_5$, py	−0.40	49
cis	Ru	$(NH_3)_4$, Cl, py	0.17	50
trans	Ru	$(NH_3)_4$, Cl, py	0.20	50
	Ru	$(NH_3)_5$, py	0.30	51
	Ru	$(NH_3)_5$, 3-CN-py	0.44	52
cis,trans	Ru	$(NH_3)_4$, $(py)_2$	0.50	51
cis	Ru	$(bpy)_2$, Cl, py	0.89	53
	Ru	$(bpy)_2$, $(py)_2$	1.25	53
	Ru	bpy, $(py)_4$	1.25	53

[a] py = pyridine; bpy = 2,2′-bipyridine.

responding to the bis(pentaammineruthenium) α,ω-dipyridyl polyenes ($\beta_{M-N} = 0.95$ eV, $\Delta\alpha_M = 0$) is marked with a plus sign.

At $\Delta\alpha_M \approx 1.1$ eV for small β_{M-N}, the contour lines for the M → L transition and the intervalence M → M transition both approach 10000 cm^{-1} and a resonance is approached. Near this resonance the interaction between these two states causes the observed bands to be near-equal mixtures of the original M → M and M → L bands, and these simple state descriptors are no longer appropriate. If one continues to use these labels, then as a resonance is crossed the identity of the states best described as "M → L" and "M → M" changes discontinuously and thus cliffs appear in the contour diagrams. Also, effective two-level models are inappropriate in this region because at least one ligand state is required to describe the basic physics of the problem. They are, however, frequently applied even in this region and give rise to discontinuous coupling constants such as that seen in Figure 8.

Increasing $\Delta\alpha_M$ makes spectroscopic experimental observations much harder because the M → L and M → M bands overlap more and the weak M → M transition could easily be lost into the tail of the M → L band. Significant band-contour changes near resonance are likely, however, and it should be possible to see two bands in the spectra again.

Substitution of the ligand field or on the pyridyl groups is expected at the simplest level to raise or lower the energy of d_π orbitals while maintaining the strength of the metal to nitrogen coupling. Thus, changes observed in the II/III reduction potential parallel changes $\Delta\alpha_M$ in the orbital energies. In Table VIII, values of the observed reduction potentials of a range of complexes with respect to the NHE are given. Large positive $\Delta\alpha_M$ values of nearly 1 V are observed for some common 2,2′-bipyridyl complexes: these complexes should have only a small energy gap between the M → L and M → M states (see Figure 8)), and a near-resonant situation could result. Such resonances would be sensitive to the value of $\Delta E_{III,II}$, and highly nonexponential or even nonmonotonic behavior could be observed.

Only a few ruthenium complexes are known with an oxidation potential lower than that of the (pyridyl)pentaammineruthenium complex, but significant energy lowering is possible by substituting osmium for ruthenium. Predictions of the properties of osmium complexes is difficult because the reorganization energy $\Delta E_{III,II}$, metal to nitrogen coupling β_{M-N}, and comproportionation constants are likely to change considerably. The energy gap $\Delta E_{III,H}$ still remains quite large, however, and one does not anticipate that complexes with exceptionally large through-bridge coupling could be produced by using osmium.

VIII. Thermal Electron Transfer

As seen in the last section, photoinduced electron-transfer processes become increasingly difficult to study as resonances are approached because, in the most interesting region, the spectral bands strongly overlap. Thermal electron-transfer processes, in which electrons are transferred with rate constant k by thermal activation over a barrier, are no more difficult to detect on-resonance than off-resonance and thus provide better opportunities for the study of fast processes. The physics of the thermal and photoinduced electron-transfer processes is shown in Figure 11. Larsson's calculation procedure[42-44] for thermal electron transfer involves a search for either a single internal coordinate (e.g., the Ru–N bond length) or some "solvent coordinates" that place a system at the top of the reactive barrier. There, the maximum mixing of the donor and acceptor wave functions occurs: the intermetallic coupling is then given simply as half of the difference between the two metal energy levels. This theory is often applied to photoinduced processes, but as Figure 11 suggests, the energy gaps to the bridge states (which involve M → L and L → M excitations) change as the nuclear coordinate at which transfer occurs changes. When the bridge states are nonresonant, the difference between ν and $\nu - \lambda/2$ in Figure 11 is unimportant and the two couplings should be very similar. Ultrafast electron-transfer processes involve near-resonant bridge states; in this case significant differences are expected between the coupling observed in thermal and photoinduced processes.

We apply the reorganizational energy correction shown in Figure 11 in order to examine the transition state's reactivity. Precise values of the rate constant k depend critically upon the interactions of the system with the solvent, and many different responses are possible,[34] including that given by Fermi's Golden rule. While the Golden Rule typically is appropriate for aqueous inorganic electron-transfer processes, in this series of papers we are concerned with a general approach that is applicable when, for example, the rate constant is significantly affected by solvent dynamics as well. A very useful general measure of k is its maximum value attainable in any solvent, k_R; this quantity is

(42) Larsson, S. *J. Chem. Soc., Faraday Trans. 2* **1983**, *79*, 1375.
(43) Larsson, S.; Volosov, A. *J. Chem. Phys.* **1986**, *85*, 2548.
(44) Larsson, S.; Broo, A.; Källebring, B.; Volosov, A. *Int. J. Quantum Chem. Quantum Bio. Symp.* **1988**, *15*, 1.

named after Rabi who first suggested an expression for it. In the Golden Rule regime, the actual rate constant is proportional to k_R^2.

Far from resonance, k_R is proportional[34] to the splitting between the metal d_π orbitals at the transition state. This interpretation of k_R involves the introduction of a two-state model, and an expression for the best possible effective coupling element $\bar{V}_{12}^{(J)}$ is given by Joachim.[36] Unfortunately, effective two-level models are inappropriate in the resonance region because they give discontinuous results; see Figures 8–10. In an earlier paper in this series (ref 34, eq 10), we introduced a model that deduces values for k (and thus k_R) without the introduction of an effective two-level model, and the results can conveniently be expressed in terms of a parameter $\bar{V}_{12}^{(J)}$. This measure of the intermetallic coupling reduces in the nonresonant limit to $\bar{V}_{12}^{(J)}$ while providing a good description of the coupling in resonance situations.

For thermal electron-transfer processes, the possibility exists that competitive reactions may reduce the overall quantum yield. This becomes likely for through-bridge electron transfer because some component of the electronic motion always leaks onto the bridge where it can remain for quite long times. If no competing chemical processes exist, then it will take a long time for the last fraction of the electron transfer to complete, thus effectively slowing the electron-transfer rate. If, on the other hand, competitive reactions occur, then these long-time components will not contribute to the primary electron-transfer reaction, and so the reaction will appear to be completed faster. Quantum yield is taken into account by using a parameter σ[34] that damps out contributions from weak components to k. We report in detail calculations with $\sigma = 0$ (no damping, full quantum yield) and some calculations with $\sigma = 0.1/2^{1/2}$ (small but nonzero).

For the $n = 0$ ligand, four molecular orbitals have no component on the nitrogen atoms and thus do not contribute to the electron transfer. As n increases, the reduced symmetry allows some involvement of these orbitals to occur, but the effects are minor. We thus simplify the thermal electron-transfer problem by excluding these orbitals from the calculation. This avoids numerical problems for the very weakly coupled orbitals of the $n = 1$ complex.

Contour diagrams of the average bridge-length dependence γ and the exponential ζ are given in Figure 12 on the basis of the thermal couplings $\bar{V}_{12}^{(J)}$ and $\bar{V}_{12}^{(R)}$ (for $\sigma = 0$). These results correspond to the photoinduced results shown in Figure 9 and 10. Values of the couplings appropriate for the bis(pentaammineruthenium) α,ω-dipyridyl polyenes are given in Table VII, and here results are given for both $\sigma = 0$ and $\sigma = 0.1/2^{1/2}$. We see that the absolute value of $\bar{V}_{12}^{(R)}$ is quite sensitive to the quantum yield, with the values at $\sigma = 0.1/2^{1/2}$ expected to correspond best to the results of a typical experiment. Compared to the couplings seen for the photoinduced process, the $\sigma = 0.1/2^{1/2}$ couplings are 15%–50% weaker and decay faster and more exponentially with increasing bridge length. These effects arise because, in the asymmetric configuration, the Ru^{III} level is very close to the ligand LUMO level (see Figure 2), while at the saddle point this distance is greatly increased. As a consequence, the metal d_π orbital energy must be raised 0.6 eV higher in order to enter a resonance region of thermal electron transfer. Thus, complexes such as the $(bpy)_2$ complexes described in Table VII will be near-resonant in optical experiments but somewhat removed from resonance in thermal experiments.

Away from resonances, the results for γ and ζ shown in Figure 12 are quite similar. As resonances are crossed, $\bar{V}_{12}^{(J)}$ is discontinuous while $\bar{V}_{12}^{(R)}$ smoothly links the different branches of $\bar{V}_{12}^{(J)}$. At high $|\beta_{M-N}|$, the metal atom couples strongly to the bridge nitrogen atoms, and a resonance situation is entered so that $\bar{V}_{12}^{(J)}$ differs significantly from $\bar{V}_{12}^{(R)}$. Such high couplings are unlikely for metal–ligand complexes but are possible in other electron-transfer systems such as π-coupled organic free radicals or in σ-coupled ring systems in which the Peierls distortion is negligible (see ref 45 and references therein).

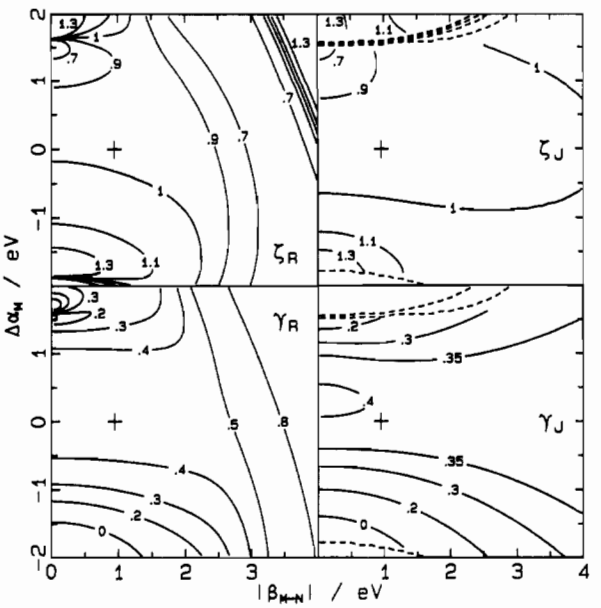

Figure 12. Contours of the exponentiality parameter ζ and the decay constant γ evaluated from $\bar{V}_{12}^{(R)}$ ($\sigma = 0$) and $\bar{V}_{12}^{(J)}$ over $n = 0$–4 for thermal electron transfer as functions of the metal to nitrogen interaction strength β_{M-N} and the change in the d_π energies $\Delta\alpha_M$ (eq 16). Discontinuities in $\bar{V}_{12}^{(J)}$ caused by resonances are marked by dashed lines.

IX. Hückel Calculations

It might be asked whether one could use Hückel-type Hamiltonian (e.g., as in refs 36 and 41) to represent all of the electronic interactions. As discussed in section I, a problem with this approach is that it contains too many uncontrolled parameters that are adjusted simply to give agreement between theory and a particular experiment. As emphasized by Salem,[26] these parameters are not unique and rarely one set of parameters can describe more than one experiment. Thus, we do not know a priori which set of Hückel parameters is appropriate for which purpose.

Long-distance electron-transfer problems are very sensitive to the size of the band gap between the bridge occupied and virtual orbitals, as well as to the placement of the donor and acceptor orbitals within the band gap. Thus, any Hückel model must describe this band gap correctly in order to give *reliable* (rather than just *accurate*) predictions for electron-transfer rates. We find that a set of Hückel parameters that give very similar results to the results obtained with our model are $\beta_{C-C} = -3.32$ eV, $\beta_{C=C} = -4.05$ eV, $\beta_{C-C} = -2.59$ eV, $\beta_{C-N} = -3.65$ eV, $\beta_{M-N} = -0.95$ eV, $\alpha_N - \alpha_C = -1.66$ eV, and $\alpha_M - \alpha_C = 0.61$ eV. Here, the difference between the single- and double-bond strengths $\beta_{C=C} - \beta_{C-C}$ is selected to ensure that the observed $\pi \rightarrow \pi^*$ frequency is reproduced as $n \rightarrow \infty$.[26,46] Of course, it is possible by varying these parameters to force a Hückel calculation to mimic any kinetic data, and indeed it is not difficult to find sets of parameters that fit exactly the observed intermetallic couplings shown in Table VII.

X. Conclusions

The M → L and M → M bands (with the exception of the $n = 2$ M → M band) are all easily fitted, and the results show a simple progression from $n = 0$ to $n = 2$. Theory predicts the correct M → L transition moment for $n = 0$ but fails to account for the increase in intensity seen as n increases: this intensity arises as a trade-off between increasing dipole length and decreasing nitrogen coefficient on the LUMO orbital. Deconvolution of the $\pi \rightarrow \pi^*$, L → M, and L → M* bands is easy for the $n = 1$ and 2 complexes but not obvious for the $n = 0$ and pyridyl complexes. The $\pi \rightarrow \pi^*$ band is seen to move to lower frequency as n increases and as the bis(metal) oxidation state increases. It becomes more intense as n increases but is stronger in the Ru^{II}–Ru^{II} form of $n = 0$ and in the Ru^{III}–Ru^{III} form of $n = 1$ and $n = 2$. Both the

(45) Gaudiello, J. G.; Kellog, G. E.; Tetrick, S. M.; Marks, T. J. *J. Am. Chem. Soc.* **1989**, *111*, 5259.

(46) Dewar, M. J. S. *J. Chem. Soc.* **1952**, 3544.

$\pi \rightarrow \pi^*$ transition intensity and frequency are overestimated by theory: a more detailed CNDO calculation for the ligands themselves including configuration interaction alleviates these problems. The L → M band moves to lower frequency and becomes broader and more intense as n increases.

In general, test results obtained with ab initio ligand molecular orbitals do not differ significantly from results obtained with CNDO. Both methods provide a similar description of the molecular orbital coefficients and of the occupied orbital energies; CNDO calculates the virtual orbital energies at considerably lower energy with smaller spacings, however. Since CNDO is parametrized to provide a good description of the spectroscopy of these molecules, one presumes that its energy levels, when used in conjunction with the simple approximations used herein, are more appropriate than the ab initio levels in this application. Quantitatively, the calculated spectra are quite similar independent of the method used to determine the ligand molecular orbitals. The major difference between the CNDO and ab initio spectra is that the ab initio calculations place much less intensity into the L → M* and M → L* bands and place these bands at higher energy when $n > 0$. Also, it is shown that an appropriate parametrization for the Hückel method can be constructed that leads to quite similar results. From a philosophical perspective, however, it is desirable to use a calculation method that contains no adjustable parameters at all. We are presently looking into ways of adapting programs like CNDO/S–CI[29] and Xα[47] to handle solvent effects and/or second-series transition metals.

The analysis presented for the spectra of the Ru^{III}–Ru^{III} complexes shows unambiguously that a triplet ground state is dominant for these ions at room temperature. Note that symmetry lowering of the singlet state as a result of the torsional motions cannot account for the observed spectra because the ligands, at their most probable configurations, retain enough symmetry to uphold the selection rules displayed in Figure 3.

Because of the uncertainty in the interpretation of the experimental M → M spectrum for $n = 2$, it is not possible to conclude from experiment the nature of the distance dependence of the intramolecular coupling; the experimental results, however, are not inconsistent with the postulate of exponential decay of the coupling with increasing bridge length. Spectra of the highest quality are necessary in order to test out the present theories for long-distance electron-transfer reactions. It is also necessary to take into account effects such as floppy torsional motions, and experimental systems should be designed to control conformation as tightly as is possible.

Theory predicts that the electronic coupling decreases almost exponentially with distance and predicts complexes that will show much slower, less exponential bridge-length dependences. Synthesis of these complexes is of interest because of possible applications to molecular electronic devices,[48] but by nature it will be difficult to deconvolve the intervalence M → M spectra from the overlapping M → L spectra.

The effective coupling seen between the metal orbitals is a function of the nuclear coordinates. This is contrary to the usual notion of electronic spectroscopy that the electronic coupling is largely coordinate independent and arises from the coordinate dependence of the energy gaps of the bridge states that transmit the coupling. Far from resonance between the bridge and the metal states, this effect is not important, but it is very important near resonance regions. It gives rise to different coupling strengths depending upon whether the electron is transferring by thermal or photoinduced mechanisms.

Acknowledgment. We wish to thank Prof. H. Taube (Stanford), Prof. P. Ford (University of Santa Barbara), and Prof. T. J. Meyer (The University of North Carolina) for their helpful discussions and further information on published and unpublished spectral data, Dr. G. B. Bacskay (University of Sydney) for performing the ab initio calculations, and Prof. S. Sternhell, Dr. L. Field, and Dr. P. A. Lay (all of University of Sydney) for stimulating discussions. J.R.R. is indebted to the Australian Research Council for the provision of a Research Fellowship.

(47) Zhang, L. T.; Ko, J.; Ondrechen, M. J. *J. Am. Chem. Soc.* **1987**, *109*, 1666.
(48) Aviram, A. *J. Am. Chem. Soc.* **1988**, *110*, 5687.
(49) Sen, J.; Taube, H. *Acta Chem. Scand.* **1977**, *A33*, 125.
(50) Marchant, J. A.; Matsubara, T.; Ford, P. C. *Inorg. Chem.* **1977**, *16*, 2160.
(51) Matsubara, T.; Ford, P. C. *Inorg. Chem.* **1976**, *15*, 1107.
(52) Richardson, D. E. Unpublished results.
(53) Buckingham, D. A.; Sargeson, A. M. In *Chelating Agents Metal Chelates*; Dwyer, F. P., Mellor, D. P., Eds.; Academic Press: New York, 1964; p 237.

Contribution from the Department of Chemistry and Laboratory for Molecular Structure and Bonding, Texas A&M University, College Station, Texas 77843

New Niobium Complexes of Alkynes. 5. Electronic Structure and Bonding in the Tetranuclear Complex of Niobium $[Nb_4OCl_8\{(PhC)_4\}_2]^{2-}$

F. Albert Cotton* and Xuejun Feng

Received December 20, 1989

Electronic structure and bonding in a newly prepared tetranuclear complex of niobium, $[Nb_4OCl_8\{(PhC)_4\}_2]^{2-}$, are discussed on the basis of molecular orbital calculations by the Fenske–Hall method. The anion consists of a planar, rectangular Nb_4 group with an oxygen atom at the center, and a C-shaped PhC–C(Ph)C(Ph)–CPh chain clasps each short Nb–Nb edge at the middle and lies in a plane perpendicular to the Nb_4O plane. Our study has been mainly focused on the problems related to the unprecedented structural features of the anion, specifically, the Nb–Nb and Nb–O bonding, and the bonding of the C_4Ph_4 unit to the metal atoms. The resulting bonding scheme gives a satisfactory account of the structure and is consistent with the assignment of a formal oxidation state of III to the metal atoms and the existence of strong bonds between the close pairs of metal atoms.

Introduction

Dinuclear complexes of niobium and tantalum with alkynes as bridges have become familiar to us.[1,2] The compounds have discrete RCCR groups strongly bound to the metal atoms and forming bridges across the M–M bonds. The electronic structures of the molecules of this type and, especially, the bonding of alkynes to the metal dimers have been studied in detail and compared with other molecules of similar type but having different metal atoms.[3]

Recent synthetic study in this type of chemistry in this laboratory has been extended to some new niobium compounds that contain a tetranuclear anion, $[Nb_4OCl_8\{(PhC)_4\}_2]^{2-}$.[4] A schematic

(1) Cotton, F. A.; Shang, M. *Inorg. Chem.* **1989**, *29*, 508.
(2) Cotton, F. A.; Hall, W. T. *Inorg. Chem.* **1980**, *19*, 2354.
(3) Cotton, F. A.; Feng, X. Submitted for publication in *Inorg. Chem.*

0020-1669/90/1329-3697$02.50/0